# Conjugation of a Novel Apaf-1 Inhibitor to Peptide-based Cell-Membrane Transporters. Effective Methods to Improve Inhibition of Mitochondria-Mediated Apoptosis

Mar Orzáez[a], Laura Mondragón[a], Isabel Marzo[b], Glòria Sanclimens[c], Àngel Messeguer[c], Enrique Pérez-Payá[a,d], and María J. Vicent[a*]

[a] Dept. Medicinal Chemistry. Centro de Investigación Príncipe Felipe, Av. Autopista del Saler, 16. E-46013 Valencia, Spain.

[b] Dept. Biochemistry and Cellular and Molecular Biology, Universidad de Zaragoza. E-50009 Zaragoza, Spain

[c] Dept. Biological Organic Chemistry, I.I.Q.A.B.(CSIC). E-08034 Barcelona, Spain

[d] Instituto de Biomedicina de Valencia, CSIC. E-46010 Valencia, Spain.

[*] To whom correspondence should be addressed. Dr. María J. Vicent, Polymer Therapeutics Lab., Dept. Medicinal Chemistry. Centro de Investigación Príncipe Felipe, Av.. Autopista del Saler, 16, E-46013 Valencia, Spain. Phone: +34-963289680; Fax: +34-963289701; E-mail: mjvicent@cipf.es.

**Abstract**

We have early identified a family of peptoids that inhibits *in vitro* the activity of the apoptosome, a macromolecular complex that activates mitochondrial-dependent apoptosis pathways. The analysis of peptide-based cell compatible delivery systems of the most active peptoid is presented. Then, the active peptoid was fused to cell penetrating peptides (CPP) as penetratin (PEN-peptoid) and HIV-1 TAT (TAT-peptoid). PEN-peptoid showed greater cell viability and as a consequence better efficiency as apoptosis inhibitor than the TAT-peptoid. The intracellular trafficking of both inhibitors was studied by flow cytometry and confocal fluorescence microscopy. Finally, the influence of the cargo (peptoid) molecules on the conformational behavior of the CPP in buffers and in membrane mimetic environments was analyzed using circular dichroism (CD) spectroscopy.

**Keywords:** Apoptosis; apoptosome inhibitors; cell-penetrating peptides; drug delivery systems; conformational analysis, membrane mimetics.

## 1. Introduction

Apoptosis, or programmed cell death, is a key cellular mechanism involved in a broad range of physiological processes. Deregulated apoptosis is associated with several human pathologies, such as cancer, ischemic injuries and neurological disorders. Therefore, there is an increased interest in defining new pharmacological targets that could control apoptosis pathways, which in turn would offer new opportunities for the discovery and development of drugs [12, 28, 33]. In order to identify molecules that could ameliorate disease-associated apoptosis, drug discovery efforts have initially targeted caspase activity [10, 32]. However, compensatory mechanisms have been described as being able to invoke upon the inhibition of defined caspases [38]; thus, mitogenic signals from caspase-inhibited apoptotic cells may contribute to the maintenance of tissue homeostasis in healthy tissues and tumor growth under pathological conditions [30]. For this reason, the inhibition of cell death upstream of caspase activation could be a valuable point of intervention for the development of modulators of apoptosis pathways.

Apoptosome is a holoenzyme multiprotein complex formed by cytochrome c-activated Apaf-1 (apoptotic protease-activating factor), dATP and procaspase-9 [1, 15]. In this macromolecular complex, apoptosome-associated caspase-9 is activated, which in turn activates effector caspases. Recent data suggested that the inhibition of the apoptosome assembly might represent an interesting target for the development of apoptosis modulators [22, 36, 39]. In the absence of detailed structural information, the conventional methods used to identify of modulators of apoptosome have been based on indirect measurements of the cytochrome c- and dATP-induced activation of caspase-3-like activity on defined cytosolic extracts [18, 23]. Using this methodology Lademann et al. [18] have identified inhibitors of apoptosome through the screening of small

molecules using cytosolic extracts of selected cells, whilst Nguyen et al. [23] reported the identification of activators. In a different approach, Malet et al. [21] have identified direct Apaf-1 ligands that could be defined as a new structural class of apoptosome inhibitors. From this family of N-alkylglycine inhibitors, the most potent was that known as peptoid **1** (scheme 1; Malet et al [21]). In order to move one step forward, structural modifications of this compound had to be done given its poor solubility and low membrane permeability. All efforts performed on peptoid **1** to elongate the peptoid chain at either the C- or N-terminus indicated that the chemical diversity attached to the nitrogen atoms at the original hit had to be maintained. In this context, peptoid **1a** (scheme 1) showed an increased activity in relation to peptoid **1**. However, an initial examination of the ability to inhibit apoptosis in intact cells suggested that peptoid **1a** has a low capacity to cross cellular membranes. Thus, we further focused our studies on delivery systems by means of the use of adequate carriers. This approach could be addressed by the design of hybrid peptide/peptoid conjugates where the parent peptoid **1** was fused to well characterized cell penetrating peptides (CPPs) [7]. These CPPs are polybasic peptides derived from the transduction domains of certain proteins, such as penetratin (PEN), which is derived from the sequence of the Drosophila transcription factor antennapaedia [25, 35] and a 12-amino acid motif from the HIV-1 Tat protein (TAT) [4]. Fusion of a different a cargo either to PEN or TAT peptides has proven to be an efficient method for the intracellular delivery of peptides [5, 8], proteins [31], antisense oligonucleotides [2] and adenoviruses [11], among others. Nevertheless, differences between TAT and PEN membrane transport capabilities have also been observed, mainly due to the influence of the cargo. Fusion to PEN appears to be favored when using proteins with less than 100 residues, whereas TAT has been reported to be able to transduce larger molecules, including β- galactosidase (> 1000

amino acids) [31]. The carrier efficiency and the influence of the cargo of CPPs fused to small molecules have not been analyzed as much [7].

In this study we analyzed how the fusion of peptoid **1** to CPPs influence the cell membrane permeation capabilities of these carrier peptides as measured by their influence on cellular uptake, biological activity of the cargo and the correlation with the conformational properties of these molecules in the presence of synthetic lipid membranes and membrane mimetics.

## 2. Materials and methods

### 2.1. Peptide and peptide/peptoid hybrids synthesis

Penetratin (RQIKIWFQNRRMKWKK-$NH_2$) and TAT (YGRKKRRQRRRG-$NH_2$) control peptides were prepared by Fmoc-based solid phase synthesis on a 433A Applied Biosystems Peptide synthesizer. The hybrids penetratin-GG-peptoid (PEN-peptoid) and Tat-GG-peptoid (TAT-peptoid) molecules were also synthesized using the same procedure but loading the synthesizer with the pre-assembled peptoidyl **1**-resin. Peptides and conjugates were cleaved from the resin by treatment with trifluoroacetic acid (TFA, 70%) and purified by preparative RP-HPLC (Lichrospher® 100 C18, 10 μm) using different acetonitrile gradients in aqueous 0.1 % TFA. The identity and purity was confirmed by HPLC and MALDI-TOF mass spectrometry. Stock solutions of control peptides and peptide/peptoid hybrids were prepared in PBS buffer (137 mM NaCl, 2.7 mM KCl, 4.3 mM $Na_2HPO_4$, 1.4 mM $KH_2PO_4$ pH 7.3) and the concentrations were determined by UV spectroscopy and quantitative amino acid analysis.

SCHEME 1

2.2. Cell-free caspase activation assays (DEVDase activity)

A cell free system obtained from human embryonic kidney (HEK) 293 cells was used. This extract was fractioned on a Q-sepharose column that results in a fraction (named F1) enriched in endogenous Apaf-1 and a flow-through fraction (named FT) that contains cytochrome c and caspases, thus separating the components needed for caspase-9/3 activation. In a typical experiment, recombinant Apaf-1 [21] (rApaf-1; 5-10 ng) was incubated at 30 ºC by 60 min in the absence or in the presence of inhibitors and then combined with a 5 μL aliquot of FT extract, 1 mM dATP and further incubated at 37 ºC by 30 min. Then, a 3 μL aliquot was mixed with 200 μL of caspase assay buffer (PBS, 10 % glycerol, 0.1 mM EDTA, 2 mM DTT) containing 20 μM Ac-DEVD-afc (Biomol). Caspase activity was continuously monitored following the release of fluorescent afc at 37 ºC using a Wallac 1420 Workstation ($\lambda_{exc}$= 400 nm; $\lambda_{em}$= 508 nm). DEVDase activity was expressed as percentage of the initial fluorescence signal value obtained in the absence of inhibitor when the inhibitory activity of compounds was evaluated.

2.3. MTT cell viability assays

An MTT cell viability assay was used to measure cell recovery of U937 human histiocytic lymphoma cells and Saos-2 human osteosarcoma cells. Cells were seeded in sterile 96-well microtitre plates at a seeding density of $4x10^5$ and $10^5$ cells/mL, respectively and allow settling for 24 h. Doxycycline (2 μg/mL in PBS) for Saos-2 cells and doxorubicin (0.25 μg/mL in PBS) in the case of U937 cells, were then added and after 30 min peptide/peptoid **1** hybrids (0.2 μm filter sterilized) were also added to give a final concentration of 1-20 μM. After 19 h incubation time, MTT (20 μL of a 5 mg/mL solution) was added to each well, and the cells were further incubated for 5 h (a

total of 24 h incubation with the inhibitors was therefore studied). After removal of the medium, the precipitated formazan crystals were dissolved in optical grade DMSO (100 μL), and the plates were read at 570 nm using a Wallac 1420 Workstation.

2.4. Caspase activation assays in cellular models (DEVDase activity).

Cell extracts were prepared from cells seeded in 3.5 cm plates at $24x10^5$ cells per plate for U937. After different treatments, cells were harvested and the pellets re-suspended in 30 μL of extraction buffer (50 mM PIPES, 50 mM KCl, 5 mM EDTA, 2 mM $MgCl_2$, 2 mM DTT supplemented with protease inhibitor cocktail from Sigma) and kept on ice 5 min. After 3 rounds of freeze and thaw, cell lysates were centrifuged for 5 min at 14000 rpm and supernatants were collected. Quantification of total protein concentration from these cell extracts was performed using the bicinchoninic acid method. Aliquots with appropriate protein content were mixed with 200 μL of caspases assay buffer (PBS, 10 % glycerol, 0.1 mM EDTA, 2 mM DTT) containing 20 μM Ac-DEVD-afc. Caspase activity was continuously monitored following the release of fluorescent afc at 30 ºC using a Wallac 1420 Workstation ($\lambda_{exc}$= 400 nm; $\lambda_{em}$= 508 nm). DEVDase activity was expressed as either as increase of relative fluorescence units per min (ΔFU/min) or as percentage of the initial fluorescence signal value.

2.5 Cellular internalization studies by flow cytometry and confocal fluorescence microscopy.

2.5.1. Uptake of PEN-peptoid and TAT-peptoid by U-937 human histiocytic lymphoma cells.

U-937 cells were seeded in 6-well plates at a density of 1 x $10^6$ cells/mL (1 mL cell suspension per well) and allowed to settle for 24 h. Carboxyfluoresceine (CF)

labeled conjugates (CF-PEN-peptoid and CF-TAT-peptoid, both 1 μM) were added and the cells incubated for 0 to 60 min at 37 ºC. At each sample time, cells were placed on ice, the cell suspension removed and then centrifuged at 4 ºC (600 x g for 10 min). The cell pellet was re-suspended in ice-chilled PBS (5 mL), this washing procedure was repeated three times and finally the cell pellet was re-suspended in ice-chilled PBS (200 μL) and collected in falcon tubes. Cell-associated fluorescence was then analyzed using a Cytomics FC 500 (Beckman Coulter Inc.) equipped with an argon laser (488 nm) and emission filter for 530 nm. Data collection involved 25,000 counts per sample and the data were analyzed with Beckman Coulter CXP software. Data are expressed by plotting the shift in geometric mean of the entire population. Cells incubated without polymer conjugate were used to account for the background fluorescence

2.5.2. Cellular internalization of PEN-peptoid and TAT-peptoid by Saos-2 osteosarcoma cells.

For confocal microscopy internalization studies, Saos-2 cells (1 x $10^5$ cells) were seeded in glass bottom culture dishes and left to adhere to the cover slips for 24 h. Cells were incubated for either 0, 15, 30 min or 1 h at 37ºC with the CF-peptides (1 μM). After this time cells were maintained on ice, washed two times with chilled PBS and fixed with paraformaldehyde for 30 min at 37 ºC. Then cells were washed three times with PBS and the samples prepared using mounting medium for fluorescence with DAPI (Vector Lab. Inc., Burlingame). Images were captured with a confocal Leica microscope equipped with a l-blue 63 x oil immersion objective and handled with a TCS SP2 system, equipped with an Acoustic Optical Beam Splitter (AOBS). Excitation was with an argon laser (548 nm, 476 nm, 488 nm, 496 nm and 514 nm) and blue diode (405 nm). Images were captured at an 8-bit gray scale and processed with LCS software (version 2.5.1347a, Leica Germany) containing multicolor, macro and 3D components.

For live-cell imaging, Saos-2 cells (1 x $10^5$ cells) were seeded in glass bottom culture dishes and left to adhere to the coverslips for 24 h. To assess the subcellular localization of the hybrids peptide/peptoid, cells were incubated for either 15, 30 min or 1 h at 37 ºC in complete medium (1 mL) containing CF-PEN-peptoid or CF-TAT-peptoid (1 μM). Before visualization, medium containing the conjugates was removed from the cells by aspiration, and the cells were washed three times with fresh medium (37 ºC). Finally, clear complete media was added and cells were subsequently viewed for a maximum of 30 min. Images were captured with a confocal Leica microscope equipped with a l-blue 20 x objective and handled with the same system described above.

2.6. Circular dichroism (CD) measurements

CD spectra were acquired at 5 ºC on a Jasco-810 spectropolarimeter equipped with a Peltier temperature control in quartz cells of 0.1 cm path length. Peptides and hybrids were analyzed at 11 μM in all cases. CD spectra were the average of 20 scans made at 0.2 nm intervals, and always the same buffer without peptides, used as baseline, was subtracted. In the model membrane interaction studies, stock solutions of sodium dodecyl sulfate (SDS) and 1-palmitoyl-2-hydroxy-sn-glycero-3-phosphocoline (LPC) were prepared in PBS buffer. Results are expressed as mean molar residue ellipticities $[\theta]_{MR}$ (deg $cm^2$/dmol).

## 3. Results

3.1. Peptoid derivatives, PEN-peptoid and TAT-peptoid, inhibit Apaf-1 in cell extracts.

We synthesized hybrid peptide/peptoid molecules where the N-terminus of peptoid **1**, extended with two glycine residues, was fused to CPPs such as penetratin (PEN) and Tat HIV-1 (TAT) peptides which yield the compounds PEN-peptoid and TAT-peptoid,

respectively (Scheme 1). Initially, we analyzed how the fusion of peptoid **1** to the PEN and TAT peptides could affect its capability as an Apaf-1 inhibitor. Cytosolic extracts of 293 were depleted from endogenous Apaf-1 by chromatography (FT fraction) (see the Materials and methods section). When the recombinant Apaf-1 was pre-incubated with peptoid **1a** and added to this FT fraction, we observed an inhibition of caspase activity as a consequence of the inhibitory activity of peptoid **1a** on the apoptosome [21]. Using the same procedure, we analyzed the compounds PEN-peptoid and TAT-peptoid and, a compound concentration-dependent inhibition of the caspase activity was found (Figure 1). We also analyzed the synthetic peptides PEN and TAT as controls, and no inhibition was found. These results suggest that the presence of the CPPs does not modify the capability of peptoid **1** to bind to Apaf-1 and, in turn, to inhibit the apoptosome-dependent activation of caspases.

FIGURE 1

3.2. Evaluation of compound cytotoxicity and Apaf-1 inhibitory activity in cellular models.

To evaluate the biological activity of compounds the PEN-peptoid and TAT-peptoid, U937 human histiocytic lymphoma cells challenged with doxorubicin were used. In this cellular-based model, doxorubicin induces apoptosis through DNA damage and this signal is transduced to the mitochondria disturbing the mitochondrial membrane potential (MMP) and activating executioner caspases through the involvement of apoptosome. An MTT cell viability assay was initially used to evaluate the cellular toxicity of the compounds. After challenging the cells, MTT was also used to determine the prevention of cell-viability loss induced by DNA damage in U937 cells. In all cases, the TAT-peptoid showed greater cell toxicity than the PEN-peptoid

(Figure 2A), and consequently, less cell-viability recovery after challenging the cells (Figure 2B). It should be noted that treatment with 1 μM PEN-peptoid of U937 cells challenged with doxorubicin increased cell survival by 30 percent. The unspecific cell toxicity could preclude the protective effect of the compound at higher PEN-peptoid concentrations.

FIGURE 2

As a more direct indicator of apoptosis cell death, the caspase 3 activity of cells treated with the peptoid derivatives (at a concentration of 1 μM) was also analyzed using the same cellular model. A compound time-dependent inhibition of the caspase activity was found. No activity was observed with TAT-peptoid, whereas a caspase inhibition of 64 percent was found for the PEN-peptoid at 24 h. We also analyzed the synthetic peptides PEN and TAT as controls, and no inhibition was seen (data not shown).

It is well known that the apoptotic cascade can be triggered through two major pathways [16]. Extracellular signals can activate the receptor-mediated extrinsic pathway while DNA-damage, hypoxia, loss of survival and other cell stress signals trigger the mitochondrial-dependent pathway where the role of both Apaf-1 and apoptosome activation has been well established. Doxorubicin-induced apoptosis has been used in different studies [19, 27, 37], and doxorubicin was seen to induce intrinsic and extrinsic forms of apoptosis, probably through the implication of mitochondria-derived reactive oxygen species (ROS) and the modification of cell calcium homeostasis [17]. We used Saos-2 cells to obtain a more detailed analysis of the effect of the Apaf-1 ligand peptoid **1** and its related compounds in an 'only intrinsic form' of apoptosis. In this cell-based model, apoptosis is induced by the conditional expression

of Bax through the tet-ON system (Clontech). Bax is a pro-apoptotic member of the Bcl-2 family that induces apoptosis through the liberation of cytochrome c from the mitochondria; thus, the activation of apoptosis solely relies in the mitochondrial or intrinsic pathway. In the initial setup experiments with this cell system however, both PEN-peptoid and TAT-peptoid hybrids showed non specific cell toxicity, although a much smaller inhibitory activity was reached with PEN-peptoid (inhibition of caspase 3 activity: 64 % vs. 18 % in U-937 and Saos-2 cells at 24 h, respectively).

3.3 Cellular internalization studies.

In order to prove that the conjugation of our peptoid inhibitor to a CPP enhances its cellular internalization, two carboxyfluoresceine (CF) labeled derivatives (CF-PEN-peptoid and CF-TAT-peptoid) were synthesized to be used as fluorescence probes in flow cytometry and confocal fluorescence microscopy studies. Both conjugates were rapidly internalized by the cells in a time-dependent manner (with a plateau after 30 min due to fluorescence quenching – Figure 3), as observed by flow cytometry studies. It should be noticed that the TAT-peptoid showed an enhanced membrane binding propensity when compare with PEN-peptoid (fluorescence output at t = 0 min - Figure 3). Moreover, their preferred internalization mechanism seemed to be different, as seen with confocal fluorescence microscopy experiments. Whereas the PEN-peptoid showed a vesicular labeling already after a 15-minute incubation, cells incubated with the TAT-peptoid showed a cytosolic fluorescence diffusion (Figure 4). Moreover after a 1-hour incubation, the cell damage induced by the TAT-peptoid was much higher than that observed with the PEN-peptoid. This data is in good agreement with TAT-peptoid-observed cytotoxicity.

FIGURE 3 and FIGURE 4

3.4. Structural analysis by CD spectroscopy

Although PEN and TAT could be initially considered as equally efficient cell transporters for a wide variety of cargoes, the cargo could possibly influence any of the intrinsic properties of CPPs, having a direct effect on their behavior. Thus, if the cargo modifies the membrane-induced conformational transition capabilities of CPPs, these could modify cell permeability. To explore such a possibility, we analyzed the conformational behavior of both the TAT-peptoid and PEN-peptoid in membrane-mimetic environments and their respective control peptides, TAT and PEN. The CD spectra of PEN, PEN-peptoid, TAT and TAT-peptoid were initially acquired in PBS buffer at 5 ºC (Figure 5). Peptides in aqueous solution tend to be a random coil, which is a dynamic structure that changes constantly [13]. In agreement with this statement, the spectra of PEN and TAT are representative of a predominantly random structure (Figures 5B and 5C, respectivelywhilst a comparison of the CD spectra obtained for the PEN-peptoid and the TAT-peptoid suggested an influence of the cargo on the general structure of the peptide. In fact, in the absence of the CD spectrum obtained for the PEN-peptoid was representative of a β-sheet conformation and the spectrum for the TAT-peptoid was representative of a poly(proline) type II-like conformation with a CD spectrum exhibiting a weak positive band at 223 nm and a strong negative band at 196 nm [9] (Figure 5D). Trifluoroethanol (TFE) has been used as a solvent additive to explore the intrinsic ability of peptides to adopt secondary structure conformations [14]. TFE titration of PEN and PEN-peptoid solutions resulted in a substantial increase of helical content (Figures 5A and 5B), which is in good agreement with previously reported data [3]. TFE titration of the TAT peptide also induced the increase in the α-helix content (Figure 5C). For the TAT-peptoid however, a TFE-induced

conformational transition towards the partial stabilization of a mixed alpha/β secondary structure was observed. This is characterized by a CD spectrum with negative ellipticity bands at 220 nm and 205 nm and with marked intensity differences [24] (Figure 5D).

FIGURE 5

The conformational behavior of all four compounds was also analyzed in the presence of both negatively charged (SDS) or zwitterionic (LPC) membrane-mimetic environments. SDS titration of PEN induced a conformational transition towards the stabilization of a β-sheet conformation at submicellar (< 3 mM SDS concentration) and of an α-helix above the critical micellar concentration (cmc) where SDS forms micellar aggregates (Figures 6A). The PEN-peptoid showed similar trends; however, a SDS-dependent induction towards helical conformations had already occurred at submicellar concentrations. Above the cmc, the PEN-peptoid adopted a mixed alpha/beta conformation with a very intense minimum at 208 nm (Figure 6B). The TAT peptide was induced into a β-sheet conformation at submicellar SDS concentrations (Figure 6C). In the presence of micellar concentrations of SDS, the resulting CD spectrum was more difficult to analyze due to an increased tendency of the complex to precipitate out from the solution. Nevertheless, the TAT-peptoid could not be analyzed in the presence of SDS due to a non specific precipitation.

FIGURE 6

The conformational behavior of the peptides and peptide/peptoid hybrids was then studied using LPC micelles. As shown in Figures 7A and 7B, both the PEN peptide and PEN-peptoid hybrid were induced into an α-helical conformation. However, both the TAT peptide and TAT-peptoid were induced to fold into a PPII-like structure, although

the differences in the absolute intensity of the positive ellipticity band at 220 nm and the negative ellipticity band at 196 nm suggested differences in the LPC-induced conformation (Figures 7C and 7D, respectively).

FIGURE 7

## 4. Discussion

The delivery of identified therapeutics to their site of action at the correct time and concentration is a key requirement and a formidable challenge to overcome. Unfortunately, despite the promising results shown *in vitro*, most drugs have intracellular trafficking or specificity limitations to achieve the *in vivo* goal. Peptoid **1** was recently developed in our laboratories as a novel apoptosis modulator, showing great efficiency as an inhibitor of Apaf-1. However, structural modifications of this lead compound were required to overcome its poor solubility and low membrane permeability. One of the approaches taken was the synthesis of hybrid peptide/peptoid molecules where peptoid **1** was fused to the well characterized CPPs, PEN and TAT. Unexpected differences in the biological activity of the compounds were observed. PEN-peptoid showed greater cell viability and as a consequence better efficiency as an apoptosis inhibitor than the TAT-peptoid. Although both conjugates were internalized by the cells in a time-dependent manner as observed by flow cytometry studies, the preferred internalization mechanism followed by either hybrid seemed to differ, as seen with confocal fluorescence microscopy. Whereas the PEN-peptoid showed a vesicular labeling already after 15 min incubation, cells incubated with the TAT-peptoid showed a cytosolic fluorescence diffusion apart from presenting a greater membrane binding. It is tempting to speculate that under our experimental conditions, the preferred mechanism of the Saos-2 cells internalization for the PEN-peptoid is endocytosis,

whereas the TAT-peptoid shows a preferred traslocation/transduction mechanism. Moreover, after an 1-hour incubation, the cell damage induced by the TAT-peptoid was much higher than that observed with the PEN-peptoid. This data is in good agreement with the observed TAT-peptoid cytotoxicity.

The differences observed could be explained by a possible influence of the cargo (peptoid **1**) on the conformational behavior of the CPP as demonstrated by circular dichroism in aqueous solutions and in membrane mimetic environments. Although it is established that the capability of the different CPPs to adopt α-helical conformation is not an absolute requirement for internalization [6], it is accepted that different CPPs have different internalization mechanisms where the adoption of a defined peptide conformation at the aqueous/cell-membrane interface should play an important role [31, 34]. In fact, the conformational transition from unordered to α-helix was observed for both the PEN and PEN-peptoid in the presence of TFE, SDS and LPC micelles. However, some differences were observed from the analysis of the conformational transition of TAT and TAT-peptoid. In PBS solution, the control TAT peptide showed it could populate a random form while the TAT-peptoid presented PPII helix characteristics, indicating a more rigid structure which could explain the greater damage in the cell membrane as observed in microscopy studies with the FITC-TAT-peptoid**.** [13, 26]. TFE, which tended to promote secondary conformation transitions, induced an α-helix conformation on TAT, while a mixture of alpha/β–sheet secondary structures was obtained for the TAT-peptoid. It is generally accepted that when CPPs seek to interact with cell membranes, there is an initial electrostatic interaction, and afterwards, the hydrophobic amino acids have a high tendency to be allocated in the hydrophobic core. In some instances such a membrane perturbation would require local membrane reorganization probably through a transient formation of mixed peptide/lipid micelles.

The formation of such complexes could be analyzed by SDS, a membrane mimetic system that allows the study at submicellar and micellar concentrations [20]. Monomeric SDS induced a conformational change in TAT while precipitation of TAT-peptoid was observed at all the SDS concentrations analyzed, suggesting a different lipid/peptide interaction. In contrast, irrespective of the initial conformation adopted in the buffer solution, both the TAT and TAT-peptoid stabilized a PPII-like conformation in the presence of LPC micelles, although a much greater intensity of the minimum at 196 nm was observed for the TAT-peptoid (Figures 7C and 7D). These results are in partial agreement with those reported by Ruzza et al. [29] on the stabilization of a PPII conformation by the peptide TAT. These authors found that TAT could adopt a PPII conformation in a very low ionic strength buffer (Tris-HCl 5 mM, pH 6.8) and in the presence of 30 mM SDS, while we found that TAT in PBS buffer (approximately 150 mM ionic strength) adopted a random conformation and showed a tendency to stabilize α-helix, random coil and PPII-like conformations in TFE, SDS and LPC, respectively. Differences could arise from the sequence of the TAT peptide used as different regions of the TAT protein had already shown a completely different conformational behavior [13]. In their studies Ruzza et al. [29] analyzed the sequence GRKKRRQRRRPPQG. Conversely, we decided to use a shortened version (YGRKKRRQRRRG-$NH_2$) with well demonstrated cell penetrating properties [5], where the aromatic amino acid Tyr was included to allow a UV spectroscopy-based determination of peptide concentration and the Pro-Pro-Gln C-terminal residues were suppressed to facilitate the synthesis of the hybrid TAT-peptoid.

Nevertheless, the overall results suggest that the biological active conformations of both PEN and TAT could be influenced by their cargo even if such a cargo is a small molecule, and could result in a loss of the cargo expected biological activity.

Collectively, our results contribute to reinforce the observation that the selection of an appropriate carrier is a key issue with an important influence on the therapeutic efficiency of an identified drug candidate.

**Acknowledgements**

This work was supported by grants from Spanish Ministry of Science and Education (MEC) (BIO2004-998 and CTQ2005-00995), Fundación Centro de Investigación Príncipe Felipe and a Marie Curie Reintegration grant (MERG-2004-06307). Mar Orzáez thanks Bancaja for a postdoctoral fellowship. Laura Mondragón is supported by a FPI fellowship from MEC. We thank Karin Vousden (Cancer Research UK, Glasgow) for the Saos-2 cell line, Carles Mas (Parc Científic de Barcelona) for quantitative amino acid analysis and Alberto Hernández from the Confocal Microscopy Unit of the Centro de Investigación Príncipe Felipe, the confocal microscope was supported by MEC through FEDER.

## References


1 Acehan D, Jiang XJ, Morgan DG, Heuser JE, Wang XD, Akey CW. Three-dimensional structure of the apoptosome: Implications for assembly, procaspase-9 binding, and activation. Mol Cell 2002; 9: 423-432

2 Astriab-Fisher A, Sergueev D, Fisher M, Shaw BR, Juliano RL. Conjugates of antisense oligonucleotides with the Tat and antennapedia cell-penetrating peptides: Effects on cellular uptake, binding to target sequences, and biologic actions. Pharm Res 2002; 19: 744-754

3 Berlose JP, Convert O, Derossi D, Brunissen A, Chassaing G. Conformational and associative behaviours of the third helix of antennapedia homeodomain in membrane-mimetic environments. Eur J Biochem 1996; 242: 372-386

4 Brooks H, Lebleu B, Vives E. Tat peptide-mediated cellular delivery: back to basics. Adv Drug Deliv Rev 2005; 57: 559-577

5 Chen YN, Sharma SK, Ramsey TM, Jiang L, Martin MS, Baker K, Adams PD, Bair KW, Kaelin WG. Selective killing of transformed cells by cyclin/cyclin-dependent kinase 2 antagonists. Proc Natl Acad Sci USA 1999; 96: 4325-4329

6 Christiaens B, Symoens S, Vanderheyden S, Engelborghs Y, Joliot A, Prochiantz A, Vandekerckhove J, Rosseneu M, Vanloo B. Tryptophan fluorescence study of the interaction of penetratin peptides with model membranes. Eur J Biochem 2002; 269: 2918-2926

7 Dietz GPH, Bähr M. Delivery of bioactive molecules into the cell: the Trojan horse approach. Mol Cell Neurosci 2004; 27: 85-131

8 Dostmann WR, Taylor MS, Nickl CK, Brayden JE, Frank R, Tegge WJ. Highly specific, membrane-permeant peptide blockers of cGMP-dependent protein kinase I alpha inhibit NO-induced cerebral dilation. Proc Natl Acad Sci USA 2000; 97: 14772-14777

9 Fillon YA, Anderson JP, Chmielewski J. Cell penetrating agents based on a polyproline helix scaffold. J Am Chem Soc 2005; 127: 11798-11803

10 Garcia-Calvo M, Peterson EP, Leiting B, Ruel R, Nicholson DW, Thornberry NA. Inhibition of human caspases by peptide-based and macromolecular inhibitors. J Biol Chem 1998; 273: 32608-32613

11 Gratton JP, Yu J, Griffith JW, Babbitt RW, Scotland RS, Hickey R, Giordano FJ, Sessa WC. Cell-permeable peptides improve cellular uptake and therapeutic gene delivery of replication-deficient viruses in cells and in vivo. Nature Medicine 2003; 9: 357-362

12 Green DR, Kroemer G. Pharmacological manipulation of cell death: clinical applications in sight?. J Clin Invest 2005; 115: 2610-2617

13 Gregoire CJ, Loret EP. Conformational heterogeneity in two regions of TAT results in structural variations of this protein as a function of HIV-1 isolates. J Biol Chem 1996; 271: 22641-22646

14 Jayaraman G, Kumar TKS, Arunkumar AI, Yu C. 2,2,2-Trifluoroethanol induces helical conformation in an all β-sheet protein. Biochem Biophys Res Comm 1996; 222: 33-37

15 Jiang XJ, Wang XD. Cytochrome c promotes caspase-9 activation by inducing nucleotide binding to Apaf-1. J Biol Chem 2000; 275: 31199-31203

16 Jiang XJ, Wang XD. Cytochrome C-mediated apoptosis. Ann Rev Biochem 2004; 73: 87-106

17 Kalivendi SV, Konorev EA, Cunningham S, Vanamala SK, Kaji EH, Joseph J, Kalyanaraman B. Doxorubicin activates nuclear factor of activated T-

lymphocytes and Fas ligand transcription: role of mitochondrial reactive oxygen species and calcium. Biochem J 2005; 389: 527-539

18 Lademann U, Cain K, Gyrd-Hansen M, Brown D, Peters D, Jaattela M. Diarylurea compounds inhibit caspase activation by preventing the formation of the active 700-kilodalton apoptosome complex. Mol Cell Biol 2003; 23: 7829-7837

19 Liou JS, Chen JS, Faller DV. Characterization of p21(Ras)-mediated apoptosis induced by protein kinase C inhibition and application to human tumor cell lines. J Cell Physiol 2004; 198: 277-294

20 Lopez-Garcia B, Marcos JF, Abad C, Perez-Paya E. Stabilisation of mixed peptide/lipid complexes in selective antifungal hexapeptides. Biochim Biophys Acta 2004; 1660: 131-137

21 Malet G, Martín AG, Orzáez M, Vicent MJ, Masip I, Sanclimens G, Ferrer-Montiel A, Mingarro I, Messeguer A, Fearnhead HO, Pérez-Payá E. Small molecule inhibitors of Apaf-1-related caspase-3/-9 activation that control mitochondrial-dependent apoptosis. Cell Death Differ 2006; 13: 1523-1532

22 Martin AG, Fearnhead HO. Apocytochrome c blocks caspase-9 activation and Bax-induced apoptosis. J Biol Chem 2002; 277: 50834-50841

23 Nguyen JT, Wells JA. Direct activation of the apoptosis machinery as a mechanism to target cancer cells. Proc Natl Acad Sci USA 2003; 100: 7533-7538

24 Pastor MT, Lopez de la Paz M, Lacroix E, Serrano L, Perez-Paya E. Combinatorial approaches: a new tool to search for highly structured beta-hairpin peptides. Proc Natl Acad Sci U S A 2002; 99: 614-619.

25 Persson D, Thoren PEG, Lincoln P, Norden B. Vesicle membrane interactions of penetratin analogues. Biochemistry 2004; 43: 11045-11055

26 Rabanal F, Ludevid MD, Pons M, Giralt E. CD of proline-rich polypeptides: application to the study of the repetitive domain of maize glutelin-2. Biopolymers 1993; 33: 1019-1028.

27 Rebbaa A, Chou PM, Emran M, Mirkin BL. Doxorubicin-induced apoptosis in caspase-8-deficient neuroblastoma cells is mediated through direct action on mitochondria. Cancer Chem Pharmacol 2001; 48: 423-428

28 Reed JC. Mechanisms of apoptosis regulation. Cytometry 2002: 26-27 Sup 11

29 Ruzza P, Calderan A, Guiotto A, Osler A, Borin G. Tat cell-penetrating peptide has the characteristics of a poly(proline) II helix in aqueous solution and in SDS micelles. J Pept Sci 2004; 10: 423-426

30 Ryoo HD, Gorenc T, Steller H. Apoptotic cells can induce compensatory cell proliferation through the JNK and the wingless signaling pathways. Develop Cell 2004; 7: 491–501

31 Schwarze SR, Hruska KA, Dowdy SF. Protein transduction: unrestricted delivery into all cells?. Trends Cell Biol 2000; 10: 290-295

32 Scott CW, Sobotka-Briner C, Wilkins DE, Jacobs RT, Folmer JJ, Frazee WJ, Bhat RV, Ghanekar SV, Aharony D. Novel small molecule inhibitors of caspase-3 block cellular and biochemical features of apoptosis. J Pharmacol Exp Ther 2003; 304: 433-440

33 Spierings D, McStay G, Saleh M, Bender C, Chipuk J, Maurer U, Green DR. Connected to death: the (unexpurgated) mitochondrial pathway of apoptosis. Science 2005; 310: 66-67

34 Thoren PEG, Persson D, Esbjorner EK, Goksor M, Lincoln P, Norden B. Membrane binding and translocation of cell-penetrating peptides. Biochemistry 2004; 43: 3471-3489
35 Thoren PEG, Persson D, Karlsson M, Norden B. The Antennapedia peptide penetratin translocates across lipid bilayers - the first direct observation. FEBS Lett 2000; 482: 265-268
36 Wang X, Zhu S, Drozda M, Zhang WH, Stavrovskaya IG, Cattaneo E, Ferrante RJ, Kristal BS, Friedlander RM. Minocycline inhibits caspase-independent and -dependent mitochondrial cell death pathways in models of Huntington's disease. Proc Natl Acad Sci USA 2003; 100: 10483-10487
37 Wu S, Ko YS, Teng MS, Ko YL, Hsu LA, Hsueh C, Chou YY, Liew CC, Lee YS. Adriamycin-induced cardiomyocyte and endothelial cell apoptosis: In vitro and in vivo studies. J Mol Cell Cardiol 2002; 34: 1595-1607
38 Zheng TS, Hunot S, Kuida K, Momoi T, Srinivasan A, Nicholson DW, Lazebnik Y, Flavell RA. Deficiency in caspase-9 or caspase-3 induces compensatory caspase activation. Nature Med 2000; 6: 1241-1247
39 Zhu S, Stavrovskaya IG, Drozda M, Kim BYS, Ona V, Li MW, Sarang S, Liu AS, Hartley DM, Du CW, Gullans S, Ferrante RJ, Przedborski S, Kristal BS, Friedlander RM. Minocycline inhibits cytochrome c release and delays progression of amyotrophic lateral sclerosis in mice. Nature 2002; 417: 74-78

**Legends for scheme**

**Scheme 1.** Chemical structure of peptoid **1**, peptoid **1a** and the peptide/peptoid hybrids used in this study.

**Legends for Figures**

**Figure 1.** Concentration dependence inhibition of Apaf-1 mediated activation of caspases. The different peptide/peptoid hybrids and peptide controls (x axis) were analyzed at 1 μM, 5 μM, 10 μM and 20 μM (black, stripped, grey and white bars, respectively).

**Figure 2**. Evaluation of biological activity of peptoid **1** analogues. **A.** Cytotoxicity of peptoid **1a** (◆), the different peptide/peptoid hybrids (■PEN-peptoid and ● TAT-peptoid) and peptide controls (□ PEN and ○ TAT) against U937 cells measured by MTT assay after 24 h incubation. Data expressed as Mean ± SD (n>3). **B.** Evaluation of doxorubicin-induced U937 cell death inhibition by peptide/peptoid hybrids and peptide controls at different concentrations (1 μM, 5 μM, 10 μM and 20 μM (black, stripped, grey and white bars, respectively). Data expressed as Mean ± SD (n>3).

**Figure 3.** Time-dependent uptake of PEN-peptoid and TAT-peptoid in vitro by U-937 cells; panel (a) raw data collected after incubation with PEN-peptoid, (b) raw data collected after incubation with TAT-peptoid and (c) cell associated fluorescence after incubation with PEN-peptoid and TAT-peptoid. Flow cytometry analysis at 37 ºC. The values represent mean ± SEM; $n \geq 3$.

**PANELES EN MAYUSCULA Y NEGRITA O MINUSCULA Y PARENTESIS????**

**Figure 4.** Confocal microscopy live cell images of Saos-2 cells incubated at 37ºC with; PEN-peptoid for panel (a)????? 0 min, (b)?????15 min (c)???? 1 h and TAT-peptoide for panel (d) 0 min, (e)15 min, (f) 1 h Concentration 1μM.

**Figure 5.** Circular dichroism spectra in the presence of different TFE-water mixtures (▬0% TFE, □ 20% TFE, △ 50% TFE, ○ 100% TFE). **A.** PEN control. **B.** PEN-peptoid**. C.** TAT control. **D.** TAT-peptoid**.**

**Figure 6.** Circular dichroism spectra in the presence of different concentrations of SDS (▬ 0 mM SDS, □ 0.5 mM, △1 mM SDS, ○ 3 mM SDS, ◊ 11 mM SDS). **A.** PEN control. **B.** PEN-peptoid. **C.** TAT control**.**

**Figure 7.** Circular dichroism spectra in the presence of different concentrations LPC micelles (▬ 0 μM LPC, □ 100 μM LPC, △ 400 μM LPC, ○ 1000 μM LPC). **A.** PEN control. **B.** PEN-peptoid. **C.** TAT control. **D.** TAT-peptoid**.**

**Scheme 1. Orzáez et al.**

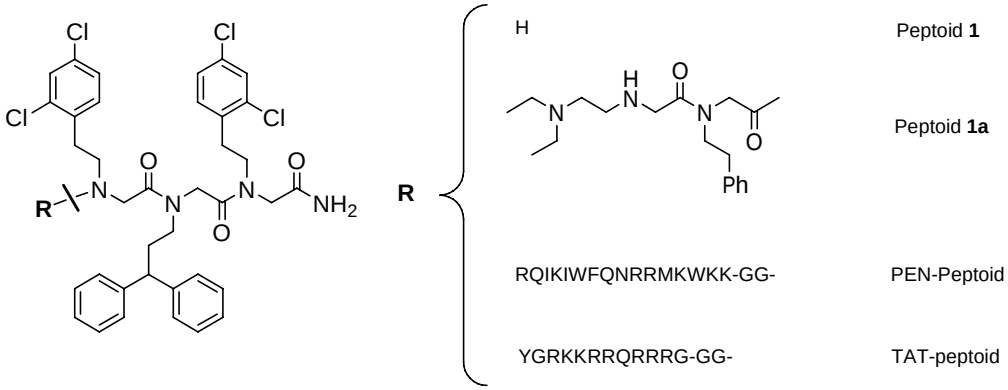

**Figure 1.** Orzáez et al.

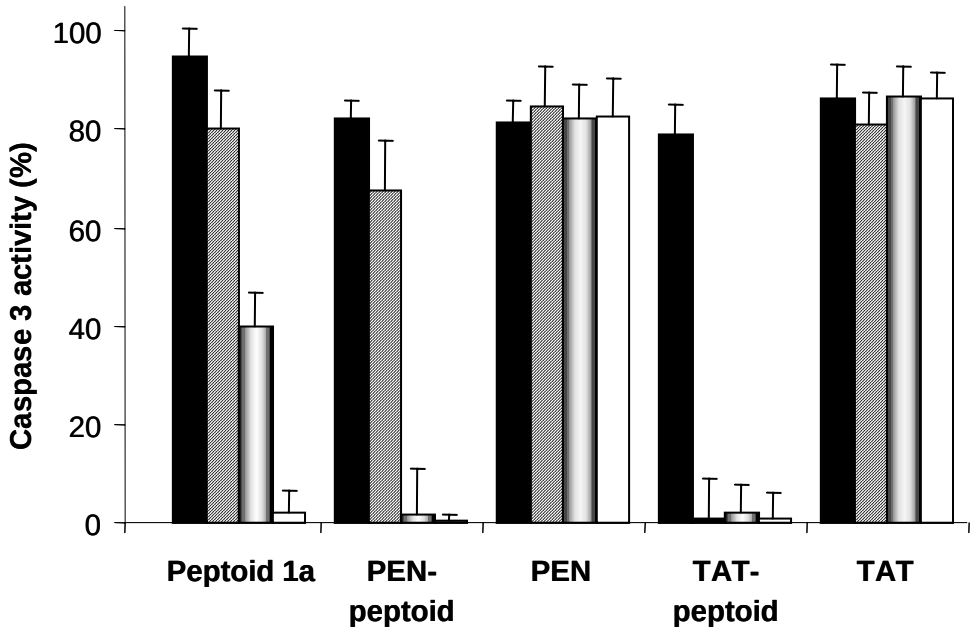

**Figure 2.** Orzáez et al.

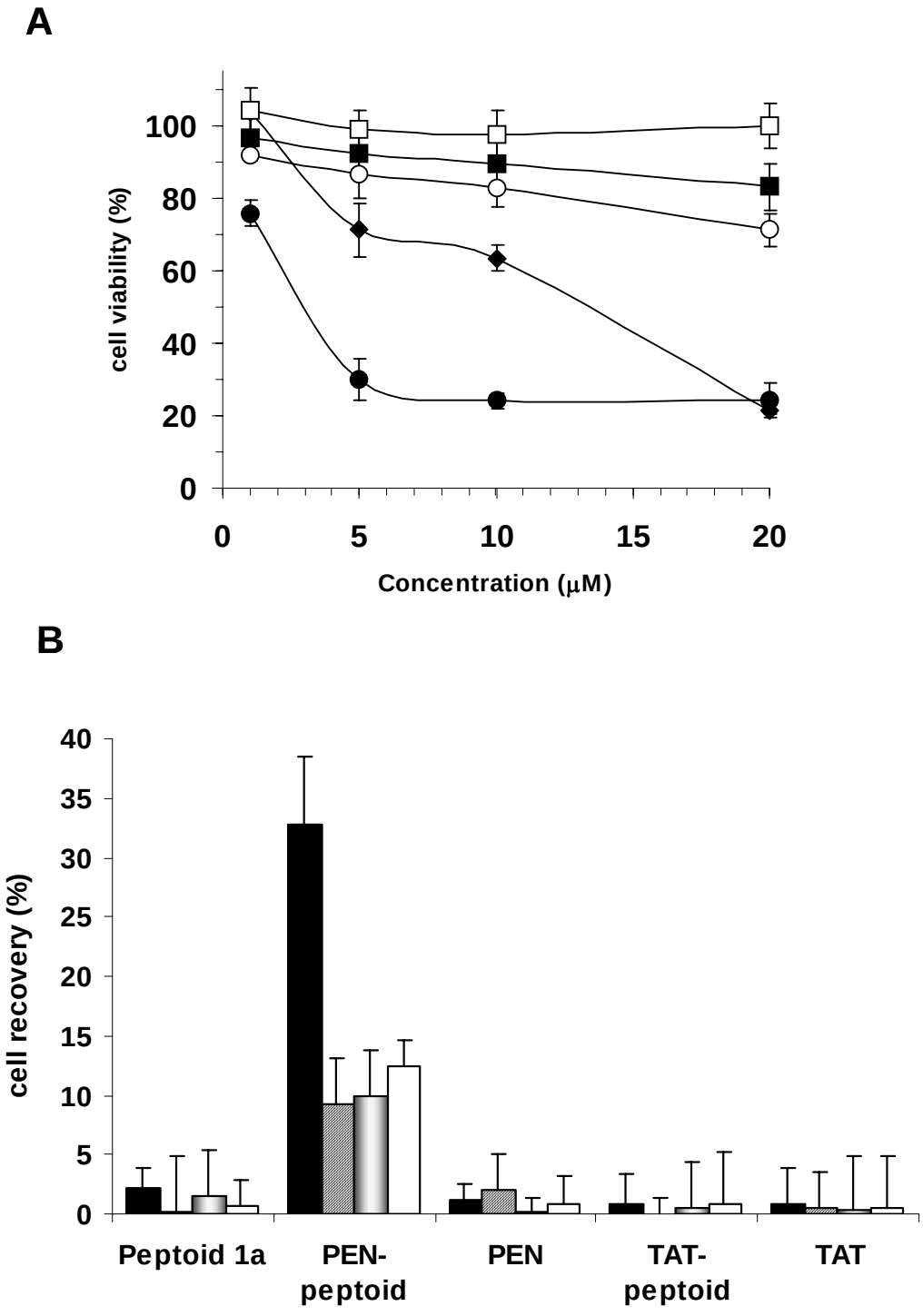

**Figure 3.** Orzáez et al.

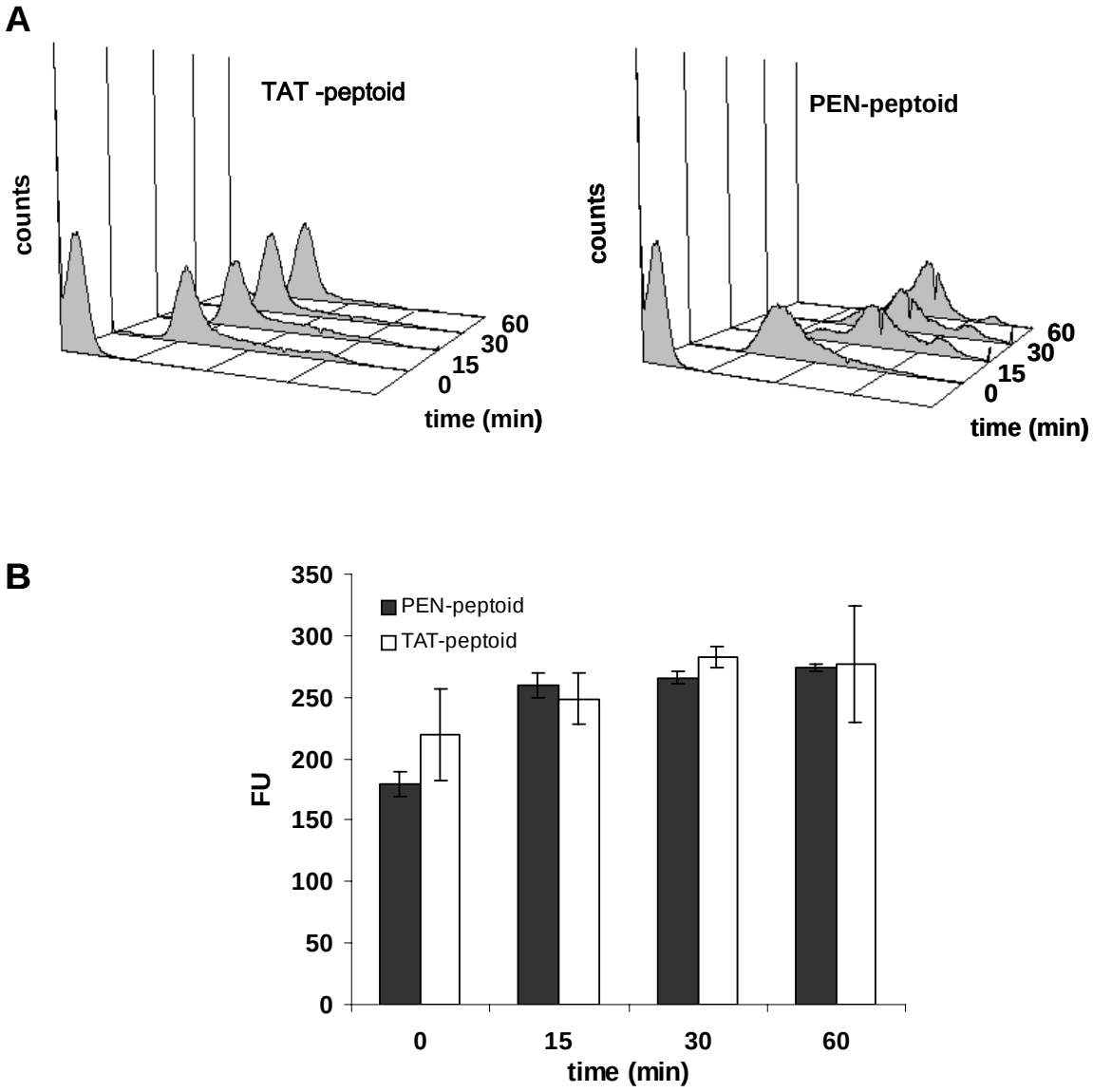

**Figure 4.** Orzáez et al. (color Figure)

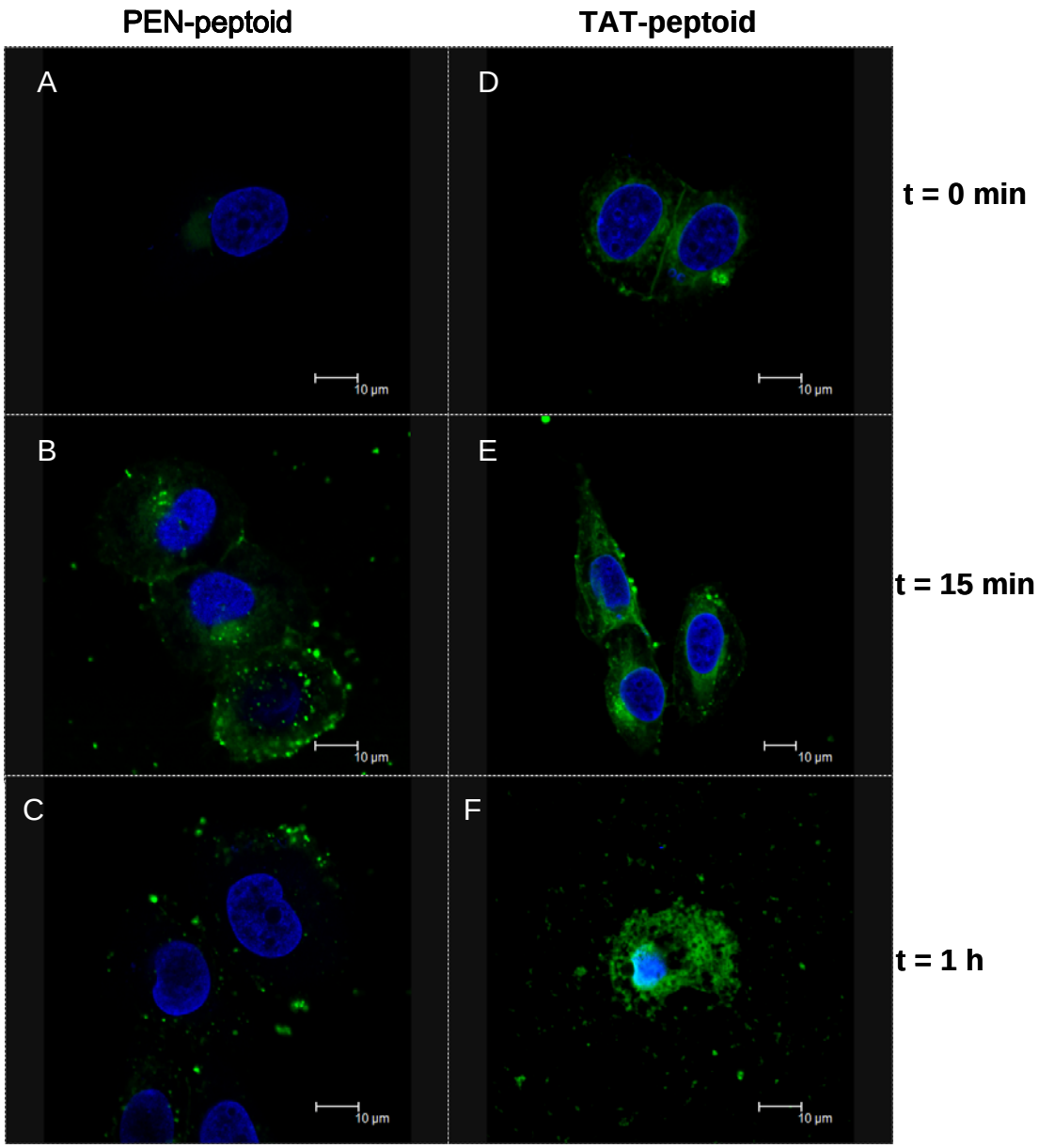

**Figure 5.** Orzáez et al.

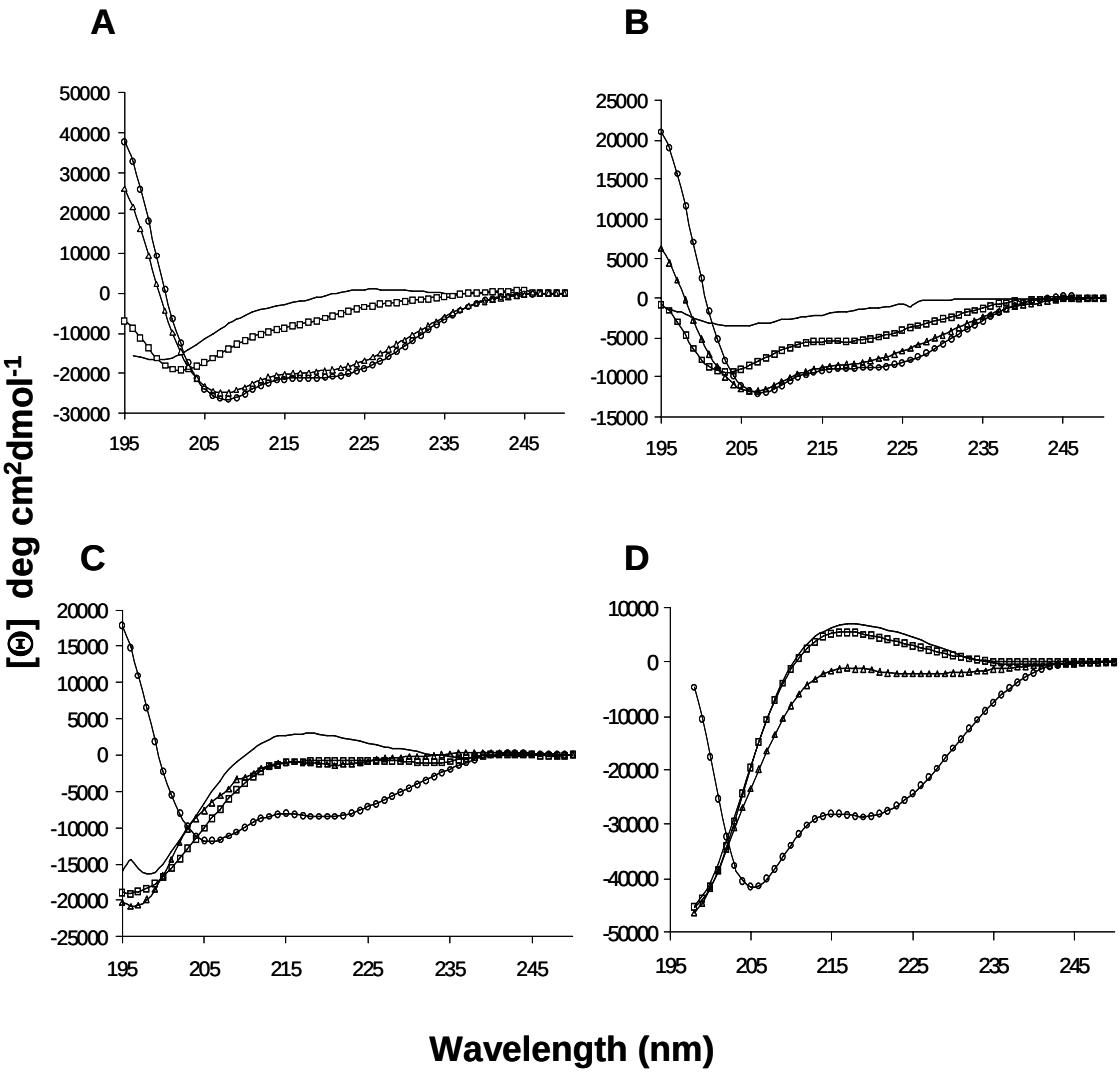

**Figure 6.** Orzáez et al.

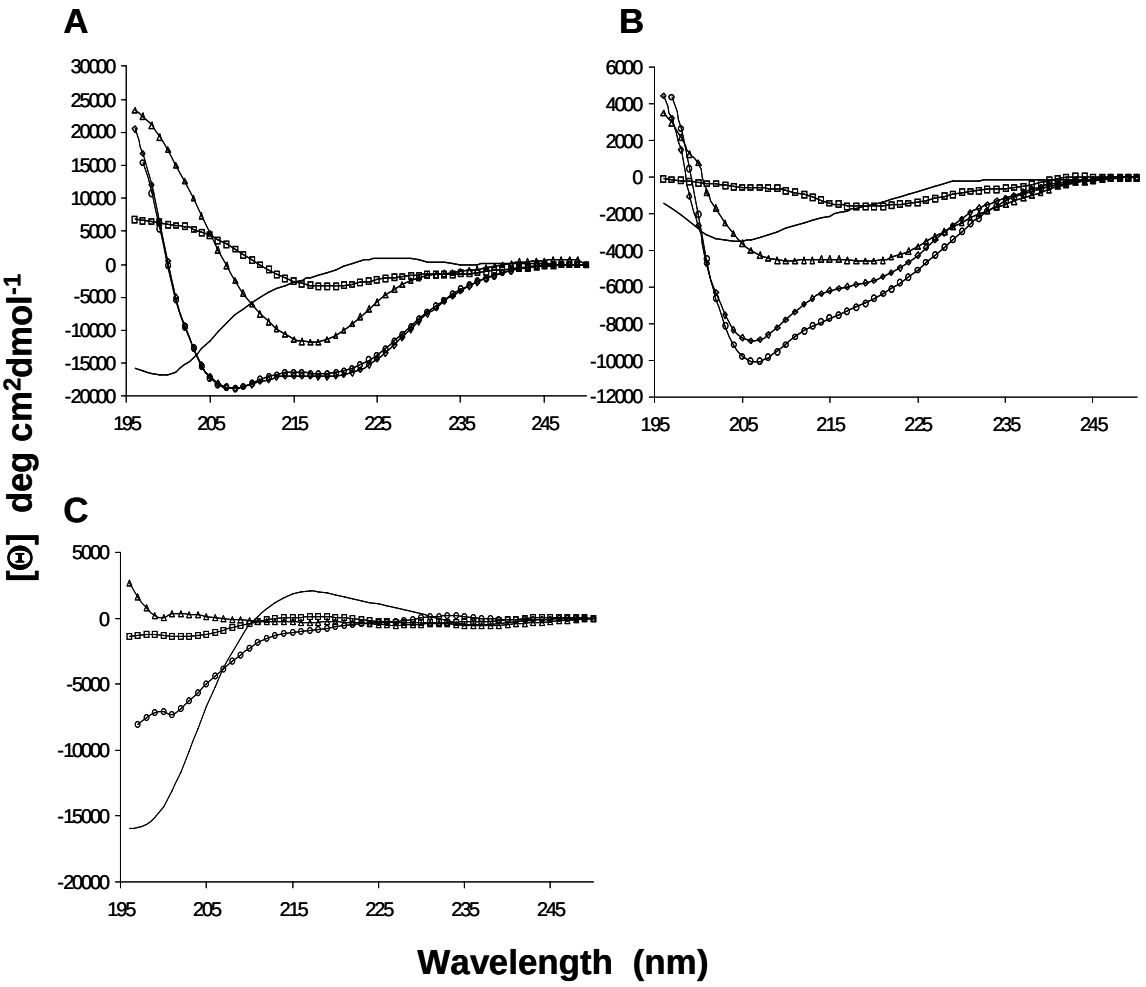

**Figure 7.** Orzáez et al.